

An improved photometric stereo through distance estimation and light vector optimization from diffused maxima region

Jahanzeb Ahmad¹, Jiulai Sun, Lyndon Smith, Melvyn Smith

Centre for Machine Vision, Bristol Robotics Laboratory, University of the West of England, Bristol, UK

Abstract

Although photometric stereo offers an attractive technique for acquiring 3D data using low-cost equipment, inherent limitations in the methodology have served to limit its practical application, particularly in measurement or metrology tasks. Here we address this issue. Traditional Photometric Stereo assumes that lighting directions at every pixel are the same, which is not usually the case in real applications, and especially where the size of object being observed is comparable to the working distance. Such imperfections of the illumination may make the subsequent reconstruction procedures used to obtain the 3D shape of the scene prone to low frequency geometric distortion and systematic error (bias). Also, the 3D reconstruction of the object results in a geometric shape with an unknown scale. To overcome these problems a novel method of estimating the distance of the object from the camera is developed, which employs photometric stereo images without using

Email addresses: jahanzeb.ahmad@uwe.ac.uk (Jahanzeb Ahmad),
jiulai2.sun@uwe.ac.uk (Jiulai Sun), lyndon.smith@uwe.ac.uk (Lyndon Smith),
melvyn.smith@uwe.ac.uk (Melvyn Smith)

¹Corresponding Author

other additional imaging modality. The method firstly identifies Lambertian diffused maxima region to calculate the object distance from the camera, from which the corrected per-pixel light vector is able to be derived and the absolute dimensions of the object can be subsequently estimated. We also propose a new calibration process to allow a dynamic(as an object moves in the field of view) calculation of light vectors for each pixel with little additional computation cost. Experiments performed on synthetic as well as real data demonstrates that the proposed approach offers improved performance, achieving a reduction in the estimated surface normal error of up to 45% as well as mean height error of reconstructed surface of up to 6 mm. In addition, when compared to traditional photometric stereo, the proposed method reduces the mean angular and height error so that it is low, constant and independent of the position of the object placement within a normal working range.

Keywords: Photometric Stereo, Light Vector Calculation, Distance Estimation.

1. Introduction

Traditional Photometric Stereo (PS) is used to recover the surface shape of an object or scene by using several images taken from the same view point but under different controlled lighting conditions [1, 2]. It was initially introduced by Woodham in 1980 [3]. PS has been extensively used in many applications especially for estimating high density local surface normals in the fields of computer vision and computer graphics. It has been used for 3D modelling [4], facial expression capturing [5, 6]. It has also been used for

9 medical applications [7, 8] and in face recognition security systems [9]. Most
10 of these applications require high accuracy reconstructed surfaces. So it is
11 critical to estimate high accuracy surface normals in order to get accurate
12 subsequent surface reconstruction from their integration. As we will show
13 in the following experiment setup, 2-3 degree error in surface normal can
14 produce up to 6 mm error in the height of reconstructed surface.

15 Current state-of-the-art systems normally assume that light sources are
16 at an infinite distance from the scene so that a homogeneous and parallel
17 incident light condition can be formed; and then the PS problem becomes
18 solvable through a group of linear equations. In reality it is not always possi-
19 ble to produce parallel(collimated) incident light, especially when the object
20 size is comparable in magnitude to the light separation and or the distance
21 of object from light source is relatively small. Any underestimation or mis-
22 alignment of the illumination may produce some error during recovery of the
23 surface normal. For example, a 1% uncertainty in the intensity estimation
24 will cause a 0.5-3.5 degree deviation in the calculated surface normal for a
25 typical three-light source photometric stereo setup [10]. Uncertainty in the
26 calibration process can also lead to systemic errors when recovering surface
27 normals and in the 3D recovered surface [11, 12].

28 Furthermore PS gives no information concerning the absolute distance of
29 the object from the camera. Other imaging modalities are normally required
30 for obtaining such range data, for example laser triangulation or stereo vision
31 techniques have been combined with the PS approach [13–17]. A dense (per-
32 pixel) surface reconstruction of a smooth and texture-less object proves to be
33 a challenging task for many range detection imaging approaches, since they

34 can only provide sparse surface data. In order to recover the range data at
35 pixel resolution, we may alternatively make use of some information about
36 the object surface itself such as convexity and smoothness.

37 In this paper we present a novel method to allow us to calculate the
38 distance of an object based on the same photometric stereo imaging setup,
39 i.e. one camera and four lights, without a requirement for any additional
40 hardware, but with little extra computation processing cost. The object's
41 distance from the camera is estimated by finding small patches on the object
42 surface whose normal is pointing towards light source. This small patch is
43 also called the diffused maxima region (DMR) and has been recently [18] used
44 for solving the problem of the generalized bas-relief ambiguity (GBR) [19].
45 The estimated distance is then used to calculate the light vectors at every
46 image pixel, thereby minimizing the error associated with the assumption
47 of a collimated light source. This approach enables the photometric stereo
48 method to effectively work with real light sources, on Lambertian surfaces
49 that have at least one patch with normal vectors pointing directly towards
50 the light source, in reality this is a reasonable assumption.

51 To the best of our knowledge we are the first to use the DMR in this
52 way, i.e. to enhance the PS method by reducing the well know problem of
53 distortion in the recovered 3D surface by improving the light vector direction
54 estimation and adding range data by using the convexity and smoothness of
55 real objects and without using other additional imaging modalities. Paper is
56 organized as following, in next section we will discuss related work after that
57 photometric stereo technique is discussed. In section 4 proposed method is
58 discussed followed by experiments and results in section 5. Finally in section

59 6 paper is concluded.

60 **2. Related Work**

61 The common low cost approach to produce collimated light is to use
62 convex lenses or concave mirrors; but even in these cases, only a narrow
63 parallel light beam with similar physical size to that of the lens or mirror can
64 be obtained. To produce a collimated light source for a larger scene area,
65 a possible solution is to develop a custom optical system with an array of
66 specially aligned individual light units. Unfortunately this results in a high
67 hardware and setup cost [20]. Another practical solution is to set the light
68 sources far away from the object[21] , so that the light can be approximated
69 as a distant radiation point source. This strategy may help to provide evenly
70 distributed radiance across the object surface, but it sacrifices the majority
71 of the illumination intensity, and correspondingly decreases the signal/noise
72 ratio of the whole system. In addition, such a distant lighting setup usually
73 means a large impractical working space is required. So this approach is
74 only suitable for those light sources able to produce high levels of energy and
75 those applications where a large redundant space is available. In terms of
76 the availability and flexibility of current commercial illumination, the distant
77 illumination solution is often not an optimal choice.

78 A nearby light source model has been considered as an alternative by Kim
79 [22] and Iwahori [23] to reduce the photometric stereo problem to find a local
80 depth solution using a single non-linear equation. By distributed the light
81 sources symmetrically in a plane perpendicular to camera optical axis, they
82 were able to get a unique solution of non-linear equations. However, selection

83 of initial values for the optimisation process and limitations in the speed for
84 solving non-linear equation are the main problems with this method.

85 A moving point light source based solution has been proposed by Clark
86 [24] termed “Active Photometric Stereo”. By moving a point light along a
87 known path close to the object surface a linear solution can be formulated to
88 solve the photometric stereo problem. However, the range of motion of light
89 must be closely controlled in order to guarantee the efficiency of the solution.

90 Kozera and Noakes introduced an iterative 2D Leap-Frog algorithm able
91 to solve the noisy and non-distant illumination issue for three light-source
92 photometric stereo [25]. Because distributed illuminators are commercially
93 available, Smith *et al.* approximated two symmetrically distributed nearby
94 point sources as one virtual distant point light source for their dynamic pho-
95 tometric stereo method [26]. Unfortunately, none of these methods lend
96 themselves to a generalized approach.

97 Varnavas *et al.* [27] implemented parallel CUDA based architecture and
98 computed light vectors at each pixel by manually placing shiny sphere at the
99 four corners of the field of view and assuming a flat plane at that distance,
100 so that a changing light direction was taken into account. However in prac-
101 tice the whole surface of the object is not flat and is not necessarily at the
102 same distance from the light source, especially when the size of the object is
103 comparable to the distance of the light source.

104 **3. Photometric Stereo**

105 According to the Lambertian reflectance model the intensity I of light
106 reflected from an object’s surface is dependent on the surface albedo ρ and

107 the cosine of the angle of the incident light as described in Equation 1. The
 108 cosine of the incident angle can also be referred as dot product of the unit
 109 vector of the surface normal \vec{N} and the unit vector of light source direction
 110 \vec{L} , as shown in Equation 2 .

$$I = \rho \cos(\phi_i) \quad (1)$$

$$I = \rho(\vec{L} \cdot \vec{N}) \quad (2)$$

111 When more than two images (four images are used in the following work)
 112 from same view point are available under different lighting conditions, we
 113 have a linear set of Equation 1 and 2 and this can be represented in vector
 114 form as shown in Equation 3.

$$\vec{I}(x, y) = \rho(x, y)[L]\vec{N}(x, y) \quad (3)$$

115 \vec{I} is the vector formed by the four pixels $((I^1(x, y), I^2(x, y), I^3(x, y),$
 116 $I^4(x, y))^T$ from four images, $[L]$ is the matrix composed by the light vec-
 117 tors $(\vec{L}^1; \vec{L}^2; \vec{L}^3; \vec{L}^4)$. Where, 1, 2, 3 and 4 is the number with respect to the
 118 individual light source direction. $[L]$ is not a square and so not invertible, but
 119 the least square method can be used to compute Pseudo-Inverse and local
 120 surface gradients $p(x, y)$ and $q(x, y)$, and the local surface normal $N(x, y)$
 121 can be calculated from the Pseudo-Inverse using Equations 4,5 and 6 where
 122 $\vec{M}(x, y) = (m_1(x, y), m_2(x, y), m_3(x, y))$.

$$\vec{M}(x, y) = \rho(x, y)N(x, y) = ([L]^T[L])^{-1}[L]^T\vec{I}(x, y) \quad (4)$$

$$p(x, y) = \frac{m_1(x, y)}{m_3(x, y)}, q(x, y) = \frac{m_2(x, y)}{m_3(x, y)} \quad (5)$$

$$N(x, y) = \frac{p(x, y), q(x, y), 1}{\sqrt{p(x, y)^2 + q(x, y)^2 + 1}} \quad (6)$$

$$\rho(x, y) = \sqrt{m_1^2(x, y) + m_2^2(x, y) + m_3^2(x, y)} \quad (7)$$

123 4. Proposed Method

124 By estimating the distance of the object from the camera we can improve
 125 the accuracy of the surface normals by calculating the light vector of every
 126 pixel based on its distance from the camera and light source. The proposed
 127 method is summarised in Pseudo code in Table 1. It is divided into three
 128 parts: “Light source position estimation”, “Object distance estimation” and
 129 “Per pixel light direction calculation”. Light source position estimation is
 130 required only once during the rig calibration process.

131 4.1. Light source position estimation

132 The general assumption that the light vector is the same at every point
 133 (pixel) is mostly not true in practice, so subsequently we use triangulation
 134 and the intersection of at least two light vectors (calculated at different posi-
 135 tions) to determine the true position of a light in a world coordinate system
 136 at the optical centre as shown in Figure 1. A specular sphere is used to calcu-
 137 late the light vectors at several (we take two as example) different locations
 138 in the imaging area. The intersection of these light vectors is taken as the
 139 position of the light in the real world coordinate system. The position of

Table 1: Pseudo code of proposed method.

<p>1. Light Source Position Estimation.</p> <p>1.1. Place a specular sphere in Field of view.</p> <p>1.2. Calculate Light vector using equation 8.</p> <p>1.3. Calculate position of highlight point in world coordinates using equation 19.</p> <p>1.4. Repeat steps 1.1 to 1.3 by placing the sphere in another location.</p> <p>1.5. Once two light vectors and two highlight positions for same light has been calculated using the above steps, the position of light can be calculated using equation 11.</p> <p>1.6. Repeat steps 1.1 to 1.5 for all light sources to calculate light positions.</p> <p>1.7. Calculate light vectors of all lights by placing the sphere in the centre of field of view by using equation 8. These light vectors will be called pseudo light vectors.</p>
<p>2. Object distance estimation.</p> <p>2.1. Capture a sequence of images of the object.</p> <p>2.2. Calculate surface normals by using pseudo light vectors and equation 6. Resultant normals are called pseudo normals.</p> <p>2.3. Calculate diffused maximum region by using equation 20.</p> <p>2.4. Create a vector from centre of diffused maximum region to centre of lens as shown in Figure 3(a).</p> <p>2.5. Now using origin of lens, pseudo light vector, position of light and vector created in step 2.4 we can calculate distance of object by using the same intersection equations as used in step 1.5.</p> <p>2.6. Repeat steps 2.2 to 2.4 for every light source and take average of all estimated distance values for final estimated value.</p>
<p>3. Per pixel light direction calculation.</p> <p>3.1. Draw an imaginary plan at the estimated distance.</p> <p>3.2. Calculate vectors from light position to every pixel on the plane to obtain per-pixel light vectors.</p>

140 light 1 is calculated by finding the intersection point of light vectors \vec{L}_1^1 and
 141 \vec{L}_2^1 as shown in Figure 1. \vec{L}_1^1 is the light vector calculated at a sphere surface
 142 position p_1^1 by placing the sphere at one random location and \vec{L}_2^1 is the light
 143 vector calculated at a sphere surface position p_2^1 by placing the sphere at an-
 144 other random location in the imaging area. To calculate \vec{L}_1^1 and \vec{L}_2^1 Equation
 145 8 is used.

$$\vec{L} = 2(\vec{n} \cdot \vec{d})\vec{n} - \vec{d} \quad (8)$$

146 Where \vec{d} is reflection direction taken as $(0, 0, 1)$, \vec{n} is unit surface normal
 147 at point p_1^1 or p_2^1 , $\vec{n} = (nx, ny, nz)$, $nx = px - cx$, $ny = py - cy$ and
 148 $n_z = \sqrt{(r^2 - n_x^2 - n_y^2)}$, (cx, cy) and (px, py) are the pixel coordinates of the
 149 sphere centre and the highlight on the sphere respectively, and r is the radius
 150 of sphere in the image plane.

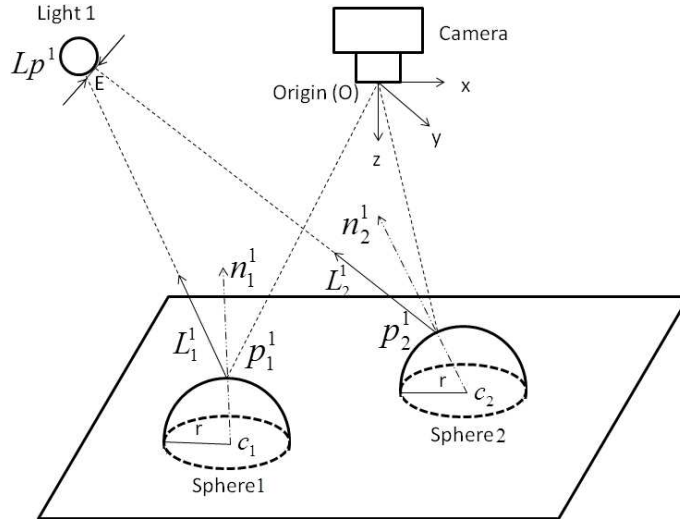


Figure 1: Calibration setup for light position calculation and initial (Pseudo) light vector calculation.

151 The intersection of \vec{L}_1^1 and \vec{L}_2^1 can be calculated using equations 9, 10 and
 152 11 [28]

$$Lp_1^1 = p_1^1 + \left(\frac{(\vec{L}_2^1 \times (p_1^1 - p_2^1)) \cdot (\vec{L}_1^1 \times \vec{L}_2^1)}{(\vec{L}_1^1 \times \vec{L}_2^1) \cdot (\vec{L}_1^1 \times \vec{L}_2^1)} \right) * \vec{L}_1^1 \quad (9)$$

$$Lp_2^1 = p_2^1 + \left(\frac{(\vec{L}_1^1 \times (p_1^1 - p_2^1)) \cdot (\vec{L}_1^1 \times \vec{L}_2^1)}{(\vec{L}_1^1 \times \vec{L}_2^1) \cdot (\vec{L}_1^1 \times \vec{L}_2^1)} \right) * \vec{L}_2^1 \quad (10)$$

$$Lp^1 = \frac{Lp_1^1 + Lp_2^1}{2} \quad (11)$$

$$E = |Lp_1^1 - Lp_2^1| \quad (12)$$

153 Lp^1 is the 3D position of light 1 in the world coordinate system. Lp_1^1 is
 154 the point on vector \vec{L}_1^1 closest to \vec{L}_2^1 , Lp_2^1 is the point on vector \vec{L}_2^1 closest
 155 to \vec{L}_1^1 , E is the distance between these two points - which can be used to
 156 measure the accuracy of the calculation. If E is zero then both light vectors
 157 intersect. However, due to error in estimating the light vector, the position
 158 of the highlight or sphere centre E is not always zero or close to zero. So we
 159 use a threshold to establish when the estimated light position is not accurate.
 160 In this case the sphere can be positioned in additional places to improve the
 161 accuracy.

162 To calculate the position of light using the above method we need the
 163 position of at least two highlights on the sphere surface. These highlights
 164 can be calculated by first calculating the centre of the sphere. As the actual
 165 size of the sphere, focal length of the camera and physical pixel size of camera

166 sensor are known, we can find the position of the centre of the sphere in the
 167 world coordinate system.

$$c(X, Y, Z) = \left[\frac{-x}{f_x} Z, \frac{-y}{f_y} Z, Z \right] \quad (13)$$

$$Z = \frac{\text{focalLength} * \text{sphereActualRadius}}{\text{pixelLength} * \text{spherePixelRadius}} \quad (14)$$

168 Where Z is the distance of sphere centre from camera in the z direction, f_x
 169 and f_y are the focal length in pixels in x and y direction. Once the centre of
 170 sphere c is known, the surface normal \vec{n} at point p (highlight pixel position)
 171 can be used to calculate p from equation 15.

$$p(X, Y, Z) = c(X, Y, Z) + k * n(X, Y, Z) \quad (15)$$

172 k is a constant required to calculate p . As p lies on the surface of the
 173 sphere $|p - c|$ should be equal to the sphere radius and by using value of p
 174 from equation 15 we can solve the value of k from the following equations.

$$|c + k\vec{n} - c| = \text{sphereActualRadius} \quad (16)$$

$$|\vec{n}| = 1 \quad (17)$$

$$k = \text{sphereActualRadius} \quad (18)$$

175 Once the value of k is calculated, it can be used in equation 15 to calculate
 176 the position of the highlight on the sphere surface in real world coordinates;
 177 as shown in equation 19.

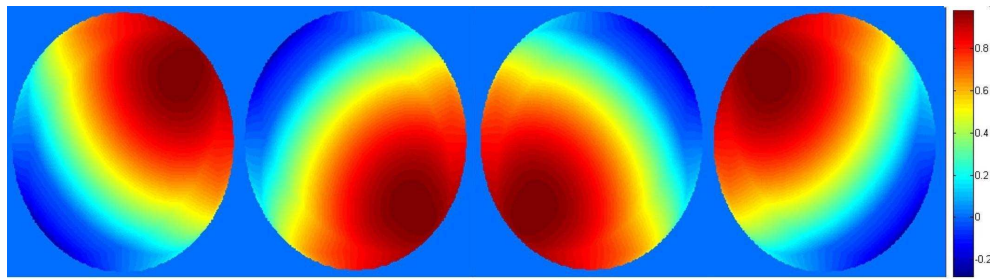
$$p(X, Y, Z) = c(X, Y, Z) + sphereActualRadius * \vec{n} \quad (19)$$

178 *4.2. Object Distance Estimation*

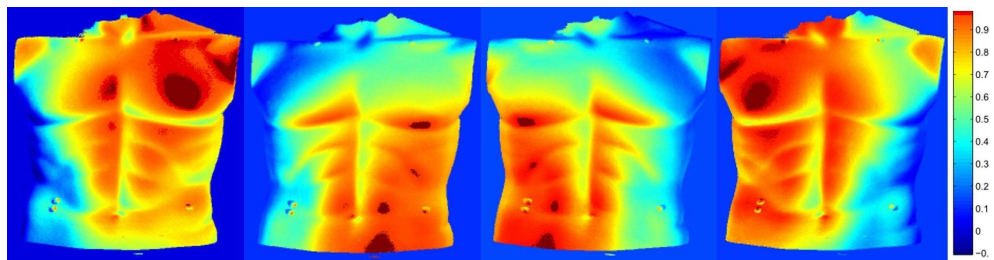
179 The object distance from the camera is calculated by using the Diffused
 180 Maxima Region (DMR), which is calculated by taking the absolute of the
 181 dot product between the pseudo light vector and pseudo surface normal, and
 182 then applying a threshold; as shown in equation 20. During experimentation
 183 we have found that for most cases the threshold is greater then or equal to
 184 0.9.

$$DMR_i = |\vec{N} \cdot \vec{L}^i| > 0.9 \quad (20)$$

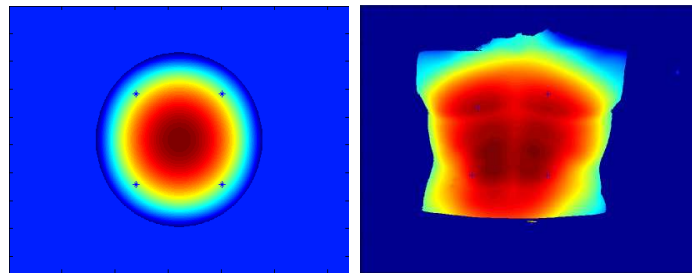
185 \vec{L}^i is a pseudo light vector for light i and \vec{N} is the pseudo surface normal
 186 at each pixel. The pseudo light vector \vec{L}^i is calculated during the calibration
 187 process by placing the sphere at the centre of the field of view, it is assumed
 188 to be same for every pixel. The centre of the *DMR* gives us the point
 189 where the surface normal and the light vector are approximately aligned.
 190 Many *DMR(s)* can exist on the surface of an object but the region with
 191 maximum pixel area is considered to be the best choice. Lights are arranged
 192 in a square arrangement as shown in Figure 4(a) and the dot product of the
 193 light vectors with surface normals are shown in Figure 2. Higher value of dot
 194 product means it is more close to diffused maxima. Figure 2 shows the four
 195 selected *DMR* centres plotted on a height map of a synthetic sphere and a
 196 real human dummy torso.



(a)



(b)



(c)

(d)

Figure 2: (a) and (b) dot product of image with its light vectors. Diffused maxima regions are in highlighted in dark red colour. (c) and (d) Diffused Maxima Regions centres are plotted on Height Map

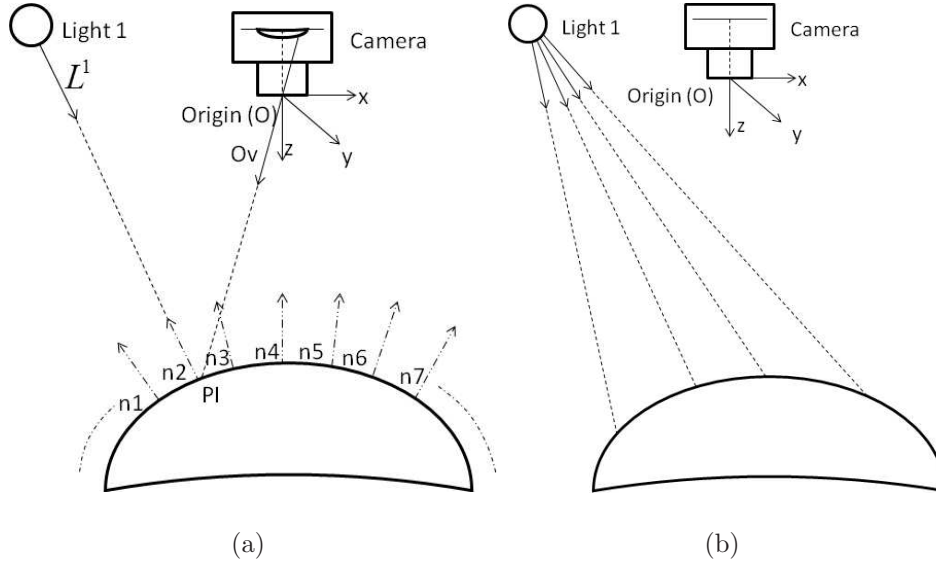


Figure 3: (a) Depth calculation using DMR and intersection of vector Ov and L^1 . (b) Light vector calculation on each point of object surface.

197 Once the *DMR* centre is identified in the image plane, a vector \vec{Ov} can
 198 be created from the *DMR* centre to the centre of the lens O , as shown in
 199 Figure 3(a). O is also the origin of the world coordinate system. Now by
 200 using origin O , position of light LP , light vector \vec{L}^1 and vector \vec{Ov} , we can
 201 determine the intersection point of these two vectors in world coordinates by
 202 using equations 9, 10 and 11. The average of the Z coordinate of these points
 203 of intersection is the estimated distance of the object from the camera.

204 4.3. Per pixel light direction calculation

205 Once the distance of the object is known from the camera, an imaginary
 206 plane parallel to the image plane is created. The pseudo height of the object
 207 is then defined relative to this plane by adding the reconstructed surface
 208 from pseudo normals; so that new light vectors for each pixel point for each

209 light are created as shown in Figure 3(b). The pseudo height of the object is
 210 calculated by integrating [29] the pseudo surface normal N and then scaling
 211 the height to compensate for the camera distance.

212 Traditional photometric stereo assumes that the light direction is same
 213 across the whole scene but in reality, particularly where the object has a
 214 comparable size to the illumination working distance, it is clear that this
 215 varies; as shown in Figure 3(b). This variation needs to be considered for
 216 accurate surface normal calculation because any variations in the illumination
 217 position are finally interpreted as uncertainty in recovered surface normals.
 218 For our synthetic imaging setup Table 2 shows the range of light vectors
 219 in terms of tilt and slant of a plane at a known distance from the camera,
 220 compared to traditional photometric stereo where the tilt and slant angle of
 221 illumination are normally assumed fixed.

Table 2: Tilt and Slant Light angle range for traditional PS and proposed method

	Our Method		Traditional PS	
	Max/Min Tilt(degree)	Max/Min Slant(degree)	Tilt (de- gree)	Slant (de- gree)
Light 1	-8.8/-76.2	83.3/57	-45	70.5
Light 2	171.2/103.8	83.4/57.2	135	70.5
Light 3	-103/-171	83/57	-135	70.5
Light 4	70.5/8.8	83/57	45	70.5

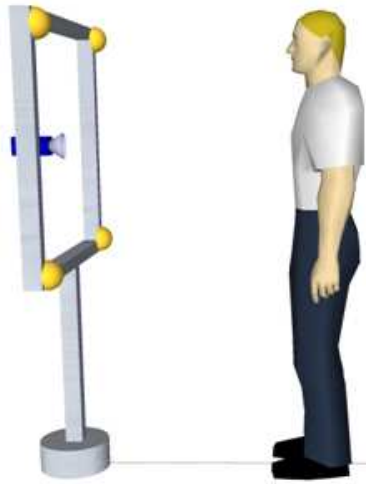
222 5. Experiments and Results

223 Experiments were performed on range of synthetic images as well as with
224 real images. For real images a setup based on a Teledyne DALSA Genie
225 HM1400 1.4 Mega pixel monochrome camera and High power LEDs was
226 designed as shown in Figure 4(a). A commercial 3dMD [30] system is used
227 to acquire ground truth data as this system has a reported 0.2 mm accuracy
228 in depth measurement.

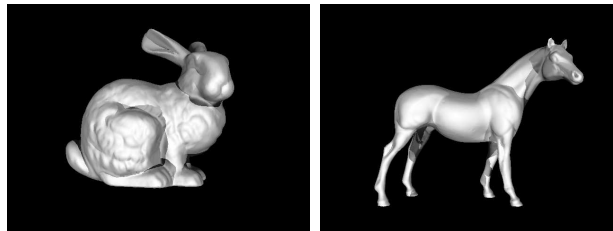
229 Figure 5(a) shows the error (mm) in the calculation of object distance
230 from camera when the initial calibration (pseudo light vectors) of the setup
231 is performed with the specular sphere located approximately at 2000mm from
232 the camera. The $\sim \pm 20$ mm uncertainty is found when the object is moved
233 from 1800mm to 2200mm from the camera. This is relatively high compared
234 to other 3D range finding technologies, however the system can achieve a
235 recovery in pixel level which is not provided by any other 3D imaging systems.

236 To test the accuracy of the surface normals acquired from the proposed
237 method we have used Mean Angular Error (MAE) as the measure of accuracy.
238 MAE is calculated by taking the cosine inverse of the dot product of a ground
239 truth surface normal and a calculated surface normal. Table 3 summaries the
240 Mean Angular error calculated from a synthetic as well as real images. Table
241 3 shows that the mean error in the height calculation of the reconstructed
242 surface is improved around 2-6 mm in height and there is around 2-3 degree
243 improvement in surface normal estimation.

244 Figure 5(b) shows mean angular error (degree) when the object is moved
245 from 1900 mm to 2100 mm with the initial light vector for traditional photo-
246 metric stereo and a pseudo light vector for our proposed method calculated

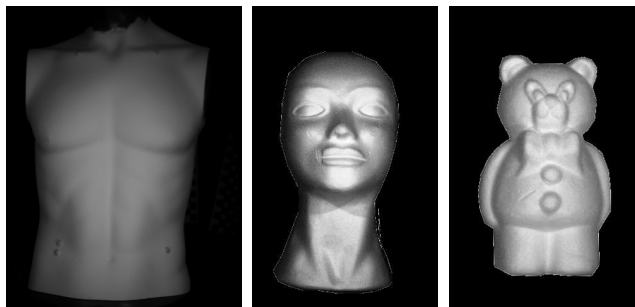


(a)



(b)

(c)

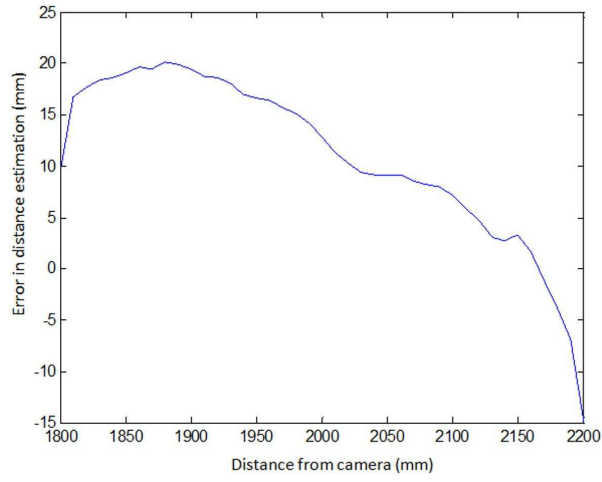


(d)

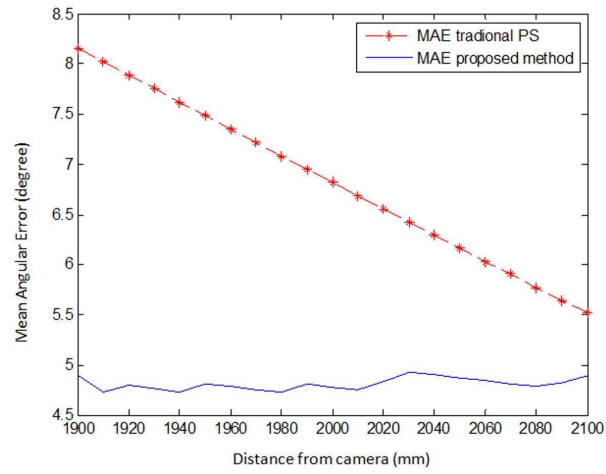
(e)

(f)

Figure 4: (a) Image acquisition Setup. (b-f) images of Objects used in Experiments



(a)



(b)

Figure 5: (a) Absolute Error in distance estimation from camera to object. (b) Mean angular error in surface normals.

247 at 2000 mm. It can be found that the MAE in traditional photometric stereo
 248 is highly dependent on the location of object with respect to the calibration
 249 position while the proposed method has a constant low MAE.

Table 3: Mean Error

	Mean Angular Error in surface normal(degree)		Mean Height Error(mm)	
	Traditional PS [3]	Our Method	Traditional PS [3]	Our Method
Synthetic Sphere	6.53	4.53	14.586	9.108
Synthetic Bunny	3.95	2.36	15.378	11.826
Synthetic Horse	3.90	2.33	9.174	6.608
Polystyrene Sphere	6.72	4.61	15.642	10.714
Human Dummy	6.88	4.86	17.006	11.066
Polystyrene Face	7.1	5.2	15.642	13.530
Polystyrene Owl	7.5	4.18	15.224	11.044

250 Figure 6(a) shows the surface reconstructed from surface normals ob-
 251 tained from traditional photometric stereo while Figure 6(b) is the surface
 252 reconstructed from surface normals obtained from the proposed method by
 253 using a Poisson based surface integrator [29]. If we visually compare Figure
 254 6(a) with the ground truth in Figure 6(c) we can easily find low frequency
 255 geometric distortion in addition to high frequency noise. This geometric
 256 distortion is due to the fact that photometric stereo in its original form in-
 257 terprets a change in light intensity due to change in light direction as change
 258 in surface normal, which is very common in low cost and large field of view

259 photometric stereo imaging setups. In comparison, Figure 6(b) is more flat
260 and closer to the ground truth. This is because the geometric distortion is
261 partially removed by considering the lighting distance from the object sur-
262 face. The same phenomena can be observed clearly by plotting slices of the
263 surfaces as shown in Figure 7.

264 Figure 7 shows slices of reconstructed surfaces. When comparing pro-
265 posed method (which estimates distance of object from the camera and cal-
266 culates light vector for every pixel using distance estimation), with traditional
267 photometric stereo (which assumes the same lighting direction for each pixel),
268 it is clear that the proposed method calculates more accurate surface normals
269 and hence better surface reconstruction.

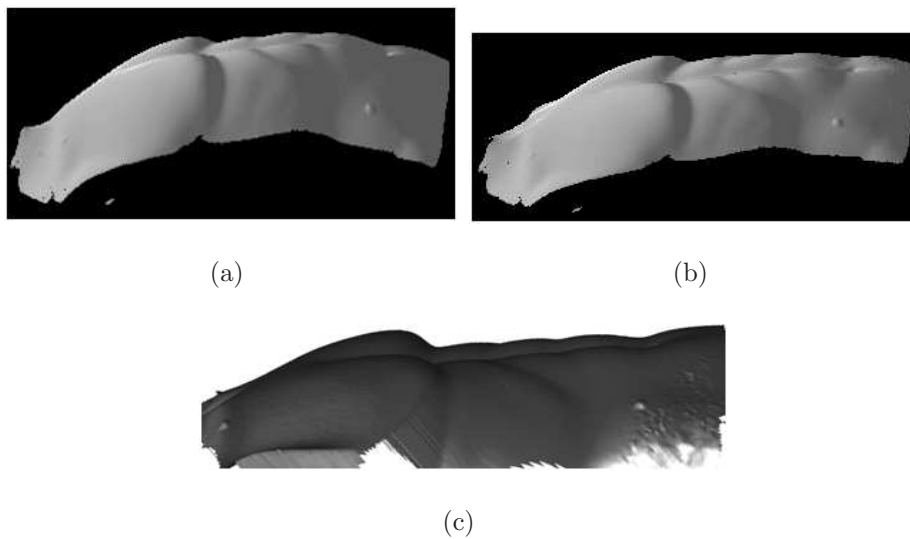


Figure 6: (a) Integrated surface using traditional PS. (b) Integrated surface using Proposed method. (c) Surface scanned from 3dMD as a ground truth.

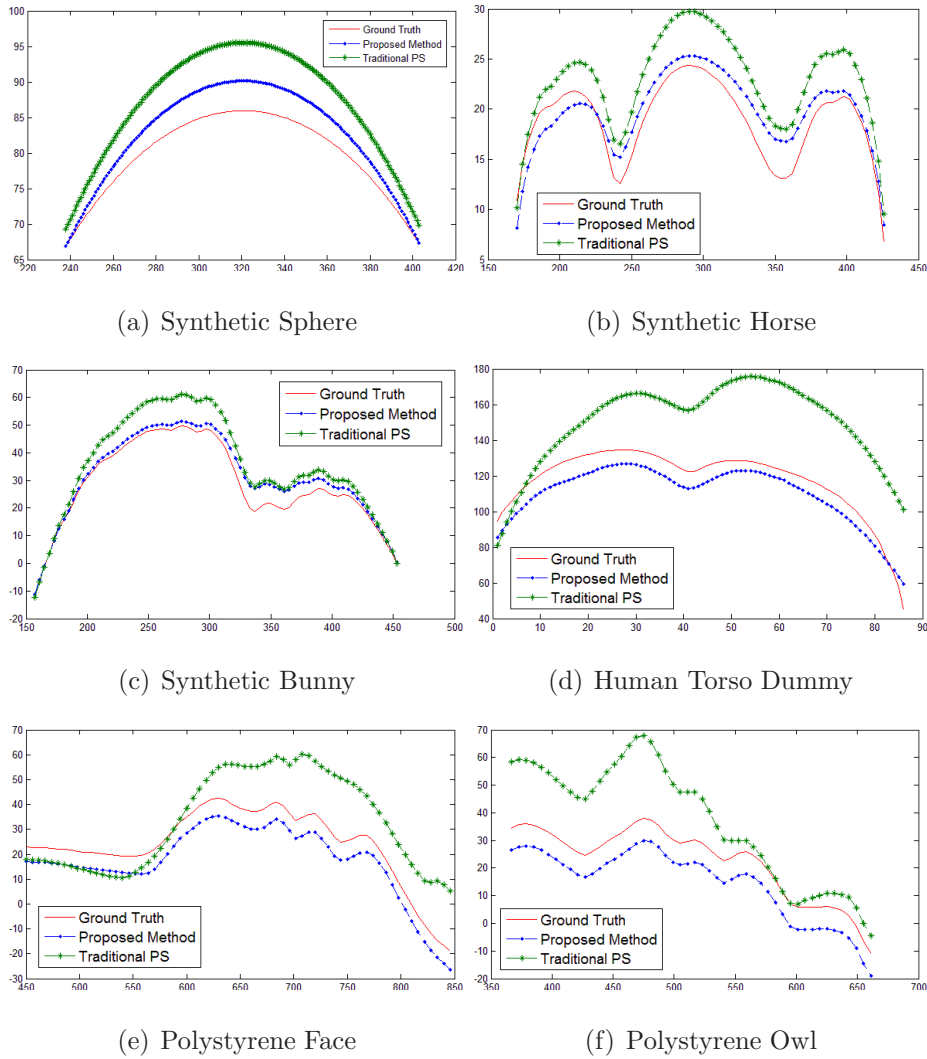


Figure 7: Slices of Integrated Surface

270 6. Conclusion

271 This approach offers a useful way to add range data, improving accuracy
 272 and reducing distortion in PS acquired reconstructed 3D surfaces. Distortion
 273 in PS derived 3D surface data is a well know limitations of the method and

274 its solution offers opportunity for taking advantage of the PS methodology
275 in a new range of challenging applications, including accurate real-time re-
276 construction non-rigid 3D surfaces, such as the moving human chest. In this
277 paper we presented a new method to calculate light vectors dynamically for
278 improving photometric stereo 3D surface reconstruction performance. The
279 improvement in light vector estimation is achieved through calculating the
280 distance of the object from the camera using diffused maxima region and then
281 using this distance to calculate per-pixel light vector dynamically. This dy-
282 namic calculation can be done in real-time (i.e. real-time reconstruction of a
283 deforming 3D shape, such as a human chest). By using the proposed method
284 the error in surface normal estimation is reduced to become almost constant
285 and independent from the working distance. Experiments performed on syn-
286 thetic and real scenes shows there is improvement of up to 45% in surface
287 normal and up to 6 mm in the reconstructed surface height.

288 **References**

- 289 [1] S. Barsky, M. Petrou, The 4-source photometric stereo technique for
290 three-dimensional surfaces in the presence of highlights and shadows,
291 IEEE Transactions on Pattern Analysis and Machine Intelligence 25 (10)
292 (2003) 1239–1252. doi:10.1109/TPAMI.2003.1233898.
- 293 [2] J. Sun, M. Smith, L. Smith, S. Midha, J. Bamber, Object surface recov-
294 ery using a multi-light photometric stereo technique for non-Lambertian
295 surfaces subject to shadows and specularities, Image and Vision Com-
296 puting 25 (7) (2007) 1050–1057. doi:10.1016/j.imavis.2006.04.025.

- 297 [3] R. Woodham, Photometric method for determining surface orientation
298 from multiple images, *Optical engineering* 19 (1) (1980) 139–144.
- 299 [4] T. Higo, Y. Matsushita, N. Joshi, K. Ikeuchi, A hand-held photometric
300 stereo camera for 3-D modeling, *IEEE 12th International Conference on*
301 *Computer Vision* (2009) 1234–1241doi:10.1109/ICCV.2009.5459331.
- 302 [5] C. Hern, G. Vogiatzis, C. Hernández, Self-calibrating a real-time monoc-
303 ular 3d facial capture system, *International Symposium on 3D Data*
304 *Processing, Visualization and Transmission (3DPVT)*.
- 305 [6] A. Jones, G. Fyffe, X. Yu, W.-C. C. Ma, J. Busch, R. Ichikari,
306 M. Bolas, P. Debevec, Head-Mounted Photometric Stereo for Perfor-
307 mance Capture, *Conference for Visual Media Production* (2011) 158–
308 164doi:10.1109/CVMP.2011.24.
- 309 [7] J. Ahmad, J. Sun, L. Smith, M. Smith, J. HENDERSON, A. MAJUM-
310 DAR, Novel Photometric Stereo Based Pulmonary Function Testing, in:
311 3rd international conference and exhibition on 3D Body Scanning Tech-
312 nologies, Lugano, Switzerland., 2012.
- 313 [8] J. Sun, M. Smith, L. Smith, L. Coutts, R. Dabis, C. Harland, J. Bam-
314 ber, Reflectance of human skin using colour photometric stereo: with
315 particular application to pigmented lesion analysis., *Skin research and*
316 *technology* 14 (2) (2008) 173–9. doi:10.1111/j.1600-0846.2007.00274.x.
- 317 [9] M. F. Hansen, G. A. Atkinson, L. N. Smith, M. L. Smith, 3D face
318 reconstructions from photometric stereo using near infrared and visible

- 319 light, *Computer Vision and Image Understanding* 114 (8) (2010) 942–
320 951. doi:10.1016/j.cviu.2010.03.001.
- 321 [10] J. Sun, M. Smith, L. Smith, A. Farooq, Examining the uncertainty of
322 the recovered surface normal in three light photometric stereo, *Image
323 and Vision Computing* 25 (7) (2007) 1073–1079.
- 324 [11] M. Kobayashi, T. Okabe, Y. Matsushita, Y. Sato, Surface Reconstruc-
325 tion in Photometric Stereo with Calibration Error, in: *International
326 Conference on 3D Imaging, Modeling, Processing, Visualization and
327 Transmission*, Inst. of Ind. Sci., Univ. of Tokyo, Tokyo, Japan, IEEE,
328 Hangzhou, China, 2011, pp. 25–32. doi:10.1109/3DIMPVT.2011.13.
- 329 [12] I. Horovitz, N. Kiryati, Depth from gradient fields and control points:
330 Bias correction in photometric stereo, *Image and Vision Computing*
331 22 (9) (2004) 681–694. doi:10.1016/j.imavis.2004.01.005.
- 332 [13] D. Junyu, G. McGunnigle, S. Liyuan, F. Yanxia, W. Yuliang, Improv-
333 ing photometric stereo with laser sectioning, *12th IEEE International
334 Conference on Computer Vision Workshops (ICCV Workshops)* (2009)
335 1748–1754doi:10.1109/ICCVW.2009.5457494.
- 336 [14] C. Hernández Esteban, G. Vogiatzis, R. Cipolla, C. Hernández, Multi-
337 view photometric stereo., *IEEE transactions on pattern analysis and ma-
338 chine intelligence* 30 (3) (2008) 548–54. doi:10.1109/TPAMI.2007.70820.
- 339 [15] H. Du, D. Goldman, S. Seitz, Binocular Photometric Stereo, in: *British
340 Machine Vision Conference 2011*, British Machine Vision Association,
341 2011, pp. 84.1–84.11. doi:10.5244/C.25.84.

- 342 [16] W. de Boer, J. Lasenby, J. Cameron, R. Wareham, S. Ahmad, C. Roach,
343 W. Hills, R. Iles, SLP: A Zero-Contact Non-Invasive Method for Pul-
344 monary Function Testing, British Machine Vision Conference 2010
345 (2010) 85.1–85.12doi:10.5244/C.24.85.
- 346 [17] C. Wu, Y. Liu, Q. Dai, B. Wilburn, Fusing multiview and photomet-
347 ric stereo for 3D reconstruction under uncalibrated illumination., IEEE
348 transactions on visualization and computer graphics 17 (8) (2011) 1082–
349 95. doi:10.1109/TVCG.2010.224.
- 350 [18] P. Favaro, T. Papadimitri, A closed-form solution to uncalibrated pho-
351 tometric stereo via diffuse maxima, in: IEEE Conference on Com-
352 puter Vision and Pattern Recognition, IEEE, 2012, pp. 821–828.
353 doi:10.1109/CVPR.2012.6247754.
- 354 [19] P. N. Belhumeur, D. J. Kriegman, A. L. Yuille, The Bas-Relief Ambi-
355 guity, International Journal of Computer Vision 35 (1) (1999) 33–44.
356 doi:10.1023/A:1008154927611.
- 357 [20] L. Smith, M. Smith, The virtual point light source model the practi-
358 cal realisation of photometric stereo for dynamic surface inspection, in:
359 Proceedings of the 13th international conference on Image Analysis and
360 Processing, ICIAP’05, Springer-Verlag, Berlin, Heidelberg, 2005, pp.
361 495–502. doi:10.1007/11553595_61.
- 362 [21] I. Ashdown, Near-field photometry: Measuring and modeling complex
363 3-d light sources, ACM SIGGRAPH95 Course Notes-Realistic Input for
364 Realistic Images.

- 365 [22] B. Kim, P. Burger, Depth and shape from shading using the photometric
366 stereo method, *CVGIP: Image Understanding* 54 (3) (1991) 416–427.
- 367 [23] Y. Iwahori, H. Sugie, N. Ishii, Reconstructing shape from shading images
368 under point light source illumination, in: *Pattern Recognition, 1990.*
369 *Proceedings., 10th International Conference on, Vol. i, 1990, pp. 83–87*
370 *vol.1.* doi:10.1109/ICPR.1990.118069.
- 371 [24] J. J. Clark, Active photometric stereo, in: *Computer Vision and Pattern*
372 *Recognition, 1992. Proceedings CVPR '92., 1992 IEEE Computer Soci-*
373 *ety Conference on, 1992, pp. 29–34.* doi:10.1109/CVPR.1992.223231.
- 374 [25] R. Kozera, L. Noakes, Noise reduction in photometric stereo with non-
375 distant light sources, *Computer Vision and Graphics* (2006) 103–110.
- 376 [26] M. L. Smith, L. N. Smith, Dynamic photometric stereo—a new technique
377 for moving surface analysis, *Image Vision Comput.* 23 (9) (2005) 841–
378 852. doi:10.1016/j.imavis.2005.01.007.
- 379 [27] A. Varnavas, V. Argyriou, J. Ng, A. A. Bharath, Dense photometric
380 stereo reconstruction on many core GPUs, 2010 IEEE Computer Society
381 *Conference on Computer Vision and Pattern Recognition - Workshops*
382 (2010) 59–65doi:10.1109/CVPRW.2010.5543152.
- 383 [28] F. Dunn, I. Parberry, 3D math primer for graphics and game develop-
384 ment, Wordware Publishing, Inc, 2011.
- 385 [29] T. Simchony, R. Chellappa, M. Shao, Direct analytical methods for solv-
386 ing Poisson equations in computer vision problems, *IEEE Transactions*

387 on Pattern Analysis and Machine Intelligence 12 (5) (1990) 435–446.
388 doi:10.1109/34.55103.

389 [30] 3dMD, www.3dmd.com/3dmdface.html.